

Consequences of a Change in the Galactic Environment of the Sun

G.P. Zank

Bartol Research Institute, University of Delaware, Newark, DE 19716

and

P.C. Frisch¹

Department of Astronomy and Astrophysics, University of Chicago, IL 60637

Received 18 November 1998; accepted 23 December 1998

arXiv:astro-ph/9901279v1 20 Jan 1999

¹Currently at the University of California, Berkeley Astronomy Department, Berkeley, California

ABSTRACT

The interaction of the heliosphere with interstellar clouds has attracted interest since the late 1920's, both with a view to explaining apparent quasi-periodic climate “catastrophes” as well as periodic mass extinctions. Until recently, however, models describing the solar wind - local interstellar medium (LISM) interaction self-consistently had not been developed. Here, we describe the results of a two-dimensional (2D) simulation of the interaction between the heliosphere and an interstellar cloud with the same properties as currently, except that the H° density is increased from the present value of $n(H^{\circ}) \sim 0.2 \text{ cm}^{-3}$ to 10 cm^{-3} . The mutual interaction of interstellar neutral hydrogen and plasma is included. The heliospheric cavity is reduced considerably in size (approximately 10 – 14 au to the termination shock in the upstream direction) and is highly dynamical. The interplanetary environment at the orbit of the Earth changes markedly, with the density of interstellar H° increasing to $\sim 2 \text{ cm}^{-3}$. The termination shock itself experiences periods where it disappears, reforms and disappears again. Considerable mixing of the shocked solar wind and LISM occurs due to Rayleigh-Taylor-like instabilities at the nose, driven by ion-neutral friction. Implications for two anomalously high concentrations of ^{10}Be found in Antarctic ice cores 33 kya and 60 kya, and the absence of prior similar events, are discussed in terms of density enhancements in the surrounding interstellar cloud. The calculation presented here supports past speculation that the galactic environment of the Sun moderates the interplanetary environment at the orbit of the Earth, and possibly also the terrestrial climate.

Subject headings: ISM — structure: ISM — general: solar system — interplanetary medium: solar system — general: stars — mass-loss: Sun — solar wind

1. Introduction

The solar system today is embedded in a warm low density interstellar cloud ($T \sim 7000$ K, $n(\text{H}^0 + \text{H}^+) \sim 0.3 \text{ cm}^{-3}$), which flows through the solar system with a relative Sun-cloud velocity of $\sim 26 \text{ km s}^{-1}$. Neutral interstellar gas penetrates the charged solar wind of the heliosphere ² – 98% of the diffuse material in the heliosphere is interstellar gas, and the densities of neutral interstellar gas and the solar wind are equal at approximately the orbit of Jupiter. The galactic environment of the Sun is regulated by the properties of the interstellar cloud surrounding the solar system. ³ However, when the surrounding cloud is of low density, the solar wind prevents most interstellar gas and dust from reaching 1 au, the location of the Earth. The discovery of small scale structure with column densities $\geq 3 \cdot 10^{18} \text{ cm}^{-2}$ in cold interstellar matter (Dieter et al. 1976, Faison et al. 1998, Frail et al. 1994, Meyer and Blades 1996, Watson and Meyer 1996, Heiles 1997), and the structured nature of the interstellar cloud surrounding the solar system, allow the possibility that the spatial density of the interstellar cloud surrounding the solar system may change within the next 10^4 – 10^6 years (Frisch 1995, 1997a, 1997b, 1998; hereafter referred to as FR). Over the past century, many conjectures have appeared in the scientific literature linking encounters with dense interstellar clouds to possible climate changes on Earth (e.g. Shapely 1921; McCrea 1975; Begelman and Rees 1976; Fahr 1968; Reid et al. 1976; McKay and Thomas 1978; Scoville and Sanders 1986; Thaddeus 1986; Frisch 1993; Bzowski et al. 1996, Frisch 1998). For these suggestions to have substance, however, it must first be shown that the interplanetary environment of the Earth varies with changing properties of the surrounding interstellar cloud. It has been shown that in the past, the galactic environment of the Sun has changed as a function of time, and that the cloud complex sweeping past the Sun now has an order-of-magnitude more nearby interstellar gas in the upwind than the downwind directions (Frisch and York 1986, FR).

²The heliopause bounds the heliosphere, which is the region of space occupied by the solar wind with a radius of roughly 100 pc minimum.

³The interstellar cloud surrounding the heliosphere is sometimes referred to as the “local interstellar cloud”, or LIC.

Therefore the sensitivity of the heliosphere to variations in the boundary conditions imposed by the LISM justify closer examination. It is the purpose of this paper to show that even a moderate alteration in the density of the cloud surrounding the solar system can yield substantial variations to the interplanetary environment in the inner heliosphere.

Early studies investigating a heliosphere embedded in a dense interstellar cloud considered the relative ram pressures of the solar wind and surrounding interstellar cloud to estimate the heliopause location (e.g. Holzer 1972, Holzer 1989). Contemporary models consider the interaction of the solar wind and interstellar medium (ISM) self-consistently, by including the effects of resonant charge exchange between the ionized and neutral gases. In the supersonic solar wind itself, charge-exchange can lead to a significant deceleration of the wind due to the freshly ionized interstellar neutrals extracting momentum from the solar wind. The concomitant reduction in solar wind ram pressure can lead to a significant reduction in the size of the heliospheric cavity. In the boundary region separating the solar wind from the ISM (the “heliosheath”), neutral hydrogen charge exchange with decelerated interstellar plasma acts to partially divert, heat and filter the H° before it enters the heliosphere. This filtration of H° in the heliosheath can reduce the number density of inflowing H° by almost half. The rather complicated nonlinear coupling of plasma and H° in the vicinity of a stellar wind is now captured in modern models (Baranov and Malama, 1993, Zank et al., 1996a, or see e.g., Zank 1998a for a review). The weak coupling of neutral hydrogen gas and plasma via resonant charge exchange affects both distributions in important ways. This implies that the self-consistent coupling of plasma and neutral hydrogen is necessary for modelling the interaction of the solar wind with the ISM. We employ a self-consistent two-dimensional (2D) numerical simulation to evaluate heliospheric structure and properties when the heliosphere is embedded in a neutral interstellar cloud whose number density is some thirty times greater than at present.

Table 1: Parameters for Current and Modelled LISM¹

	“LIC”	Solar Wind	Model	Model
	ISM	(1 au)	Plasma ISM	Neutral H ISM
$n(\text{H}^0)$ (cm^{-3})	0.2			10
$n(\text{p}^+)$ (cm^{-3})	0.1–0.25	5.0	0.1	
$n(\text{e}^-)$ (cm^{-3})	0.1–0.25	5.0	0.1	
u (km s^{-1})	26	400	–26	–26
$T(\text{K})$	7000	10^5	8000	8000
M		7.6	1.75	2.48

¹“LIC” refers to the current values of the LISM. The remaining columns list the model parameters used in the simulation. See Frisch et al. 1998 for a discussion of LIC parameters.

2. Basic Model

A multi-fluid model is used here to model the interaction of the solar wind with cloud of enhanced density. The need for modelling the neutrals as a multi-fluid stems from the variation in the charge exchange mean-free-path for H in different regions of the heliosphere and ISM. Large anisotropies are introduced in the neutral gas distribution by charge exchange with the solar wind plasma (both sub- and supersonic regions) and the multi-fluid approach represents an attempt to capture this characteristic in a tractable and computationally efficient manner. We consider the interaction of the heliosphere with an interstellar cloud similar to the cloud now surrounding the solar system, but with neutral number densities increased to 10 cm^{-3} . The parameters of the enhanced density cloud, and the solar wind at 1 au, are given in Table 1. The relatively high neutral density ensures that the H° distribution is essentially collisional. Williams et al. (1997), using the results of Dalgarno (1960), fitted the function

$$\sigma_{HH} = 3.2 \times 10^{-15} E_{eV}^{-0.11} \text{cm}^2 \quad 0.1 < E_{eV} < 100 \quad (1)$$

to describe the cross-section for H° - H° collisions (E_{eV} is the neutral atom energy in electronvolts). The collisional mean-free-path for H° with the given input parameters ranges from less than 2 au in the ISM to less than 1 au in the heliospheric boundary regions (below) to less than 2.5 au in the heliosphere itself. This suggests that the multi-fluid description outlined below is suitable on scales larger than a few au for these moderate ISM densities, and this, as illustrated below, is shown to be the case.

The heliosphere-ISM environment can be described in terms of three thermodynamically distinct regions; the supersonic solar wind (region 3), the very hot subsonic solar wind (region 2), and the ISM itself (region 1). Each region acts a source of secondary H° atoms whose distribution reflects that of the plasma distribution in the region. Accordingly, the neutral distribution resulting from the interaction of the solar wind with the surrounding interstellar cloud may be approximated by three distinct neutral components originating from each region (Zank et al. 1996a). Each of these three neutral components is represented by a distinct Maxwellian distribution function appropriate to the characteristics of the source distribution in the multi-fluid

models. This approximation allows the use of simpler production and loss terms for each neutral component. The complete highly non-Maxwellian H distribution function is then the sum over the three components,

$$f(\mathbf{x}, \mathbf{v}, t) = \sum_{i=1}^3 f_i(\mathbf{x}, \mathbf{v}, t). \quad (2)$$

In principle, for each component, an integral equation must be solved (Hall 1992; Zank et al. 1996b). Instead, Zank et al. use (2) to obtain three Boltzmann equations corresponding to each neutral component. This is an extension of the procedure developed in Pauls et al. (1995). For component 1, both losses and gains in the interstellar medium need to be included, but only losses are needed in the heliosheath and solar wind. Similarly for components 2 and 3. Thus, for each of the neutral hydrogen components i ($i = 1, 2$ or 3)

$$\frac{\partial f_i}{\partial t} + \mathbf{v} \cdot \nabla f_i = \begin{cases} P_1 + P_2 + P_3 - (\beta_{ex} + \beta_{ph})f_i & \text{region } i \\ -(\beta_{ex} + \beta_{ph})f_i & \text{otherwise} \end{cases}, \quad (3)$$

and $P_{1,2,3}$ means that the production or source term P_{ex} is to be evaluated for the parameters of components 1, 2, or 3 respectively. The β_{ex} and β_{ph} terms describe losses by either charge exchange or photoionization respectively. Under the assumption that each of the neutral component distributions is approximated adequately by a Maxwellian, one obtains immediately from (3) an isotropic hydrodynamic description for each neutral component,

$$\frac{\partial \rho_i}{\partial t} + \nabla \cdot (\rho_i \mathbf{u}_i) = Q_{\rho i}; \quad (4)$$

$$\frac{\partial}{\partial t} (\rho_i \mathbf{u}_i) + \nabla \cdot [\rho_i \mathbf{u}_i \mathbf{u}_i + p_i \mathbf{I}] = \mathbf{Q}_{m i}; \quad (5)$$

$$\frac{\partial}{\partial t} \left(\frac{1}{2} \rho_i u_i^2 + \frac{p_i}{\gamma - 1} \right) + \nabla \cdot \left[\frac{1}{2} \rho_i u_i^2 \mathbf{u}_i + \frac{\gamma}{\gamma - 1} \mathbf{u}_i p_i \right] = Q_{e i}. \quad (6)$$

The source terms Q are listed in Pauls et al. (1995) and Zank et al. (1996a). The subscript i above refers to the neutral component of interest ($i = 1, 2, 3$), ρ_i , \mathbf{u}_i , and p_i denote the neutral component i density, velocity, and isotropic pressure respectively, \mathbf{I} the unit tensor and γ ($= 5/3$) the adiabatic index.

The plasma is described similarly by the 2D hydrodynamic equations

$$\frac{\partial \rho}{\partial t} + \nabla \cdot (\rho \mathbf{u}) = Q_{\rho p}; \quad (7)$$

$$\frac{\partial}{\partial t}(\rho\mathbf{u}) + \nabla \cdot [\rho\mathbf{u}\mathbf{u} + p\mathbf{I}] = \mathbf{Q}_{mp}; \quad (8)$$

$$\frac{\partial}{\partial t} \left(\frac{1}{2}\rho u^2 + \frac{p}{\gamma - 1} \right) + \nabla \cdot \left[\frac{1}{2}\rho u^2 \mathbf{u} + \frac{\gamma}{\gamma - 1} \mathbf{u} p \right] = Q_{ep}, \quad (9)$$

where $Q_{(\rho,m,e),p}$ denote the source terms for plasma density, momentum, and energy. These terms are also defined in Pauls et al. (1995) and Zank et al. (1996a). The remaining symbols enjoy their usual meanings. The proton and electron temperatures are assumed equal in the multi-fluid models.

The coupled multi-fluid system of equations (4) – (9) are solved numerically as described in Pauls et al. (1995) and Zank et al. (1996a).

3. Simulation Results

3.1. Global Heliosphere Configuration

The global structure of the heliosphere embedded in a high density environment is obtained by integrating the coupled time-dependent system of hydrodynamic equations (4) – (6) and (7) – (9) numerically in two spatial dimensions. The integration begins at time $t=0$ using as an initial condition the heliosphere embedded in a low density cloud (Zank et al. 1996a). The LISM neutral number density is increased to 10 cm^{-3} to mimic the “encounter” of the heliosphere with a denser cloud, and it is shown below that the heliosphere then fails to settle into a steady-state or equilibrium configuration.

A time sequence of the 2D global plasma structure is illustrated in Plate 1. The time dependence of both the plasma and neutrals is presented separately below. Four successive figures are shown, each separated from the preceding in time by ~ 66 days. The color depicts the plasma temperature. The Sun is located at the origin and the interstellar wind is assumed to

Fig. 1.— Plate 1: A time sequence of the plasma temperature distribution. The color corresponds to the $\text{Log}[\text{Temperature}]$. The ordering A, B, C, D corresponds to a temporal separation from the preceding figure of ~ 66 days. The four figures show an approximately full evolutionary cycle which is repeated on a ~ 280 day period. See text for further details.

flow from the right boundary (located at 1000 au; a numerical semi-circle of radius 1000 au forms the computational domain) with the parameters listed in Table 1. Since the plasma interstellar Mach number is supersonic (see Zank et al. 1996a for a discussion about a subsonic ISM), a bow shock, labelled BS in Plate 1A, forms, which decelerates, heats and diverts the interstellar plasma around the heliospheric obstacle. The plasma is now no longer collisionally equilibrated with the interstellar H° and charge exchange between the interstellar plasma and neutrals just downstream of the bow shock leads to an effective heating/compression and diversion of the neutral interstellar H in the heliosheath region (between the bow shock and heliopause). As a result, a pile-up of decelerated, diverted and heated interstellar H° is created in the region downstream of the bow shock, which is illustrated in Plate 2. Plate 2 shows the corresponding global distribution of H° at the same times as used in Plate 1, except that the H° density is plotted. Far upstream of the bow shock, the H° number density is $\sim 10 \text{ cm}^{-3}$, increasing rapidly just downstream of the bow shock in the pile-up region with densities 2–2.5 times greater than the ambient ISM density. Changes in the neutral number density, velocity, temperature and Mach number are seen more easily in the one-dimensional (1D) plots along the stagnation axis than in Plate 2 (discussed later in the context of Figure 2). The number density of neutrals entering the heliosphere at $\sim 10 \text{ au}$ is $\sim 7 \text{ cm}^{-3}$, decreasing to $\sim 2 \text{ cm}^{-3}$ at 1 au.

The enhanced-density ISM case can be compared to simulations using the current low-density surrounding ISM (the LIC column of Table 1). The hydrogen wall of the high density cloud model possesses a more complicated structure than that of the low density case – it possesses a weak double-peaked structure along the stagnation axis in the upstream direction, reverts to a single-peaked structure away from but in the neighbourhood of the stagnation axis, after which it again becomes double-peaked. The H° flow is strongly filtered in the vicinity of the wall, this due essentially to the divergence of the H° flow through charge exchange with the bow shock-diverted interstellar plasma, thus leading to an H° number density entering the heliosphere that is much

Fig. 2.— Plate 2: A time sequence (corresponding to that of Plate 1) of the global distribution of the neutral interstellar H density. The color refers to the density measured in cm^{-3} . The hydrogen wall in the upstream direction is clearly visible, as is the effective filtration of H as it enters the heliosphere.

lower than that of the ISM.

As is well-known (e.g. Holzer 1972), the effect of interstellar H streaming through the supersonic solar wind, and experiencing charge exchange with solar wind protons, is to reduce the momentum of the solar wind significantly. The relatively large H^0 number density entering the heliosphere reduces the solar wind ram pressure significantly, 25%–75%, from its nominal non-mediated value thereby reducing the global extent of the heliosphere. For the parameters of Table 1, the heliosphere shrinks dramatically to $\sim 10 - 14$ au in the upstream direction. The density of interstellar neutral hydrogen at 1 au becomes $\sim 2 \text{ cm}^{-3}$ (Figure 2), unlike the current state for which no neutral interstellar hydrogen reaches Earth orbit (e.g. Baranov and Malama, 1993; Zank et al., 1996a). In addition, the configuration becomes unstable (see below).

The reduction in solar wind momentum is accompanied by an increase in the total temperature of the solar wind (solar wind ions plus pickup ions), in comparison to an adiabatically expanding solar wind, since pickup ions acquire a large velocity perpendicular to both the solar wind velocity and magnetic field vectors and therefore have energies that are typically ~ 1 keV in the unmediated solar wind (where $u \sim 400 \text{ km s}^{-1}$). Accordingly, beyond the ionization cavity (a cavity created by the photoionization of interstellar neutrals by solar wind UV radiation), the solar wind temperature increases (in the absence of pickup ions, the total solar wind temperature decays adiabatically, the polytropic index depending on the nature of the specific heat sources identified to heat the wind). Radial cuts along the stagnation axis for the plasma density, velocity, temperature, and Mach number are illustrated in Figure 1. The increase in the solar wind temperature is evident in Figure 1c. By contrast, in the absence of pickup ions or other heating processes, the solar wind temperature would cool adiabatically according to $r^{-4/3}$ for an adiabatic index of 5/3.

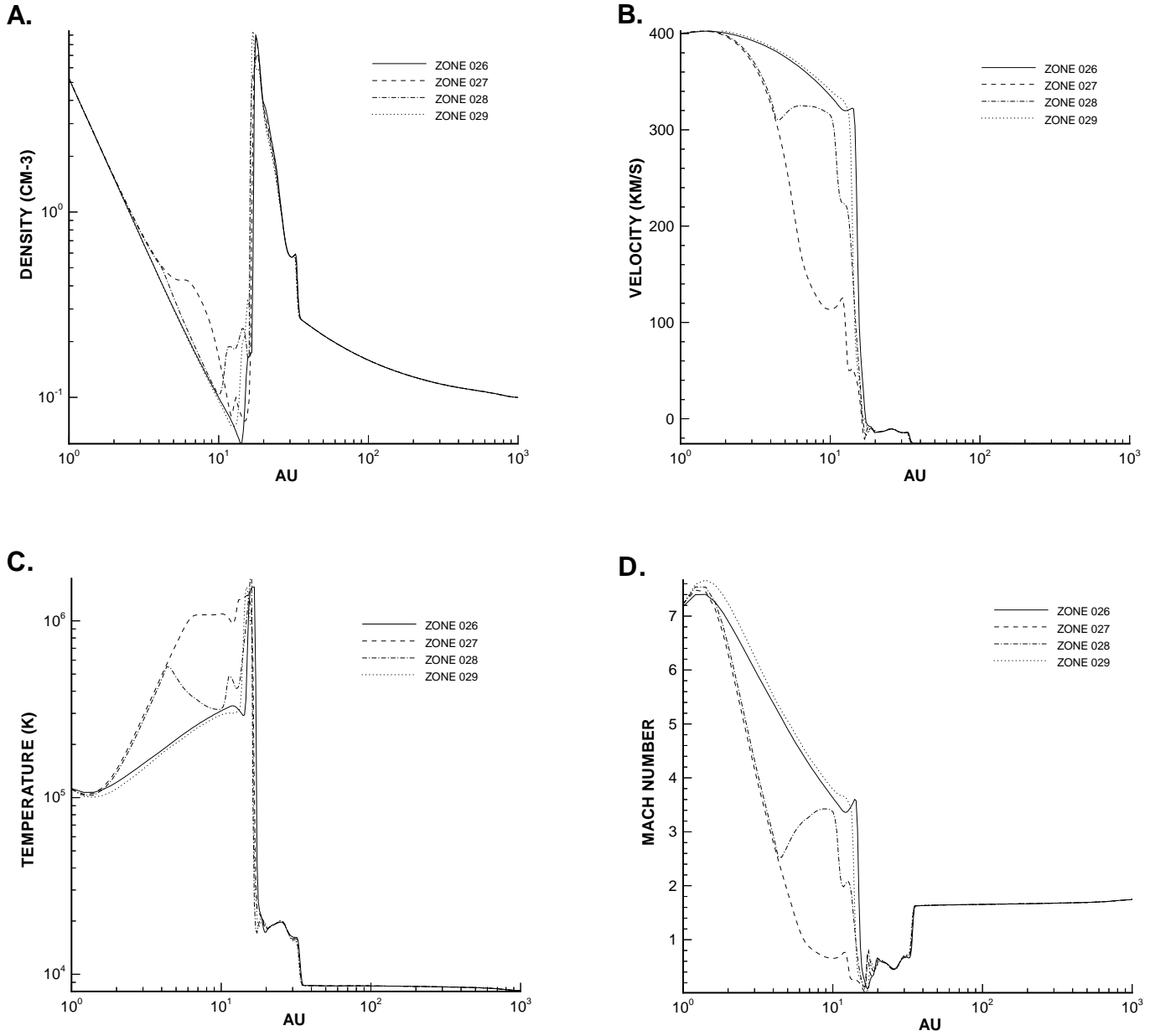


Fig. 3.— **Figure 1:** The plasma density (A), velocity (B), temperature (C) and Mach number (D) along the stagnation axis. Four curves are presented on each graph, each corresponding to a cut through one of the figures of Plate 1. In each case, the solid line corresponds to Plate 1A, the dashed line to Plate 1B, the dash-dotted line to Plate 1C and the dotted line to Plate 1D.

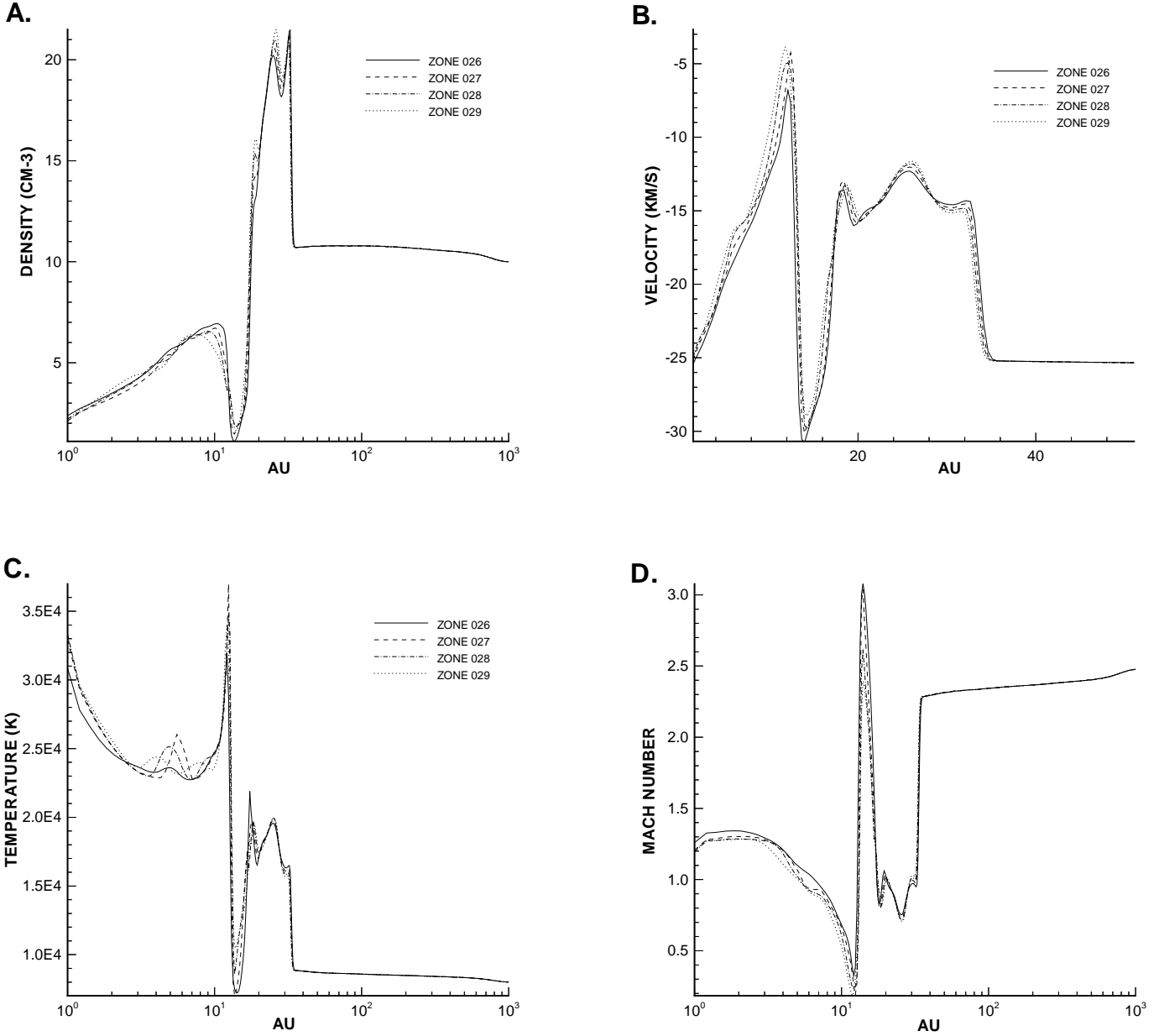


Fig. 4.— **Figure 2:** The interstellar neutral density (A), velocity (B), temperature (C) and Mach number (D) along the stagnation axis. Four curves are presented on each graph, each corresponding to a cut through one of the figures of Plate 2. In each case, the solid line corresponds to Plate 2A, the dashed to Plate 2B, the dash-dotted to Plate 2C and the dotted to Plate 2D.

3.2. Time Dependence

The very high number density of interstellar neutrals entering the heliosphere, even after filtration ($\sim 7 \text{ cm}^{-3}$, Plate 2, Figure 2a) leads to a very strong time-dependent mediation of the solar wind. In the sequence of velocity profiles plotted in Figure 1b (the sequence corresponds to the four plot sequence of Plates 1 and 2), the solar wind at the time corresponding to the solid line is decelerated from 400 km s^{-1} to $\sim 320 \text{ km s}^{-1}$ at the termination shock. Some 66 days later (the dashed line), the deceleration is considerably larger, now down to $\sim 110 \text{ km s}^{-1}$. Neutrals that were ionized and then picked up by the solar wind during the least mediated solar wind period will therefore have considerably more energy than those picked up by a strongly mediated wind (a factor ~ 10 difference). Thus, the strongly mediated solar wind will possess a very large temperature gradient. The temperature gradient can become so large that the pressure gradient, which normally decreases with increasing radial distance in weakly mediated solar wind, is now inward (Figure 3), and it is this inwardly directed pressure gradient that is responsible for decelerating the outwardly flowing solar wind so strongly. As a result of the much stronger deceleration of the solar wind, the radial solar wind density profile departs from an $\sim r^{-2}$ dependence (Figure 1a) on occasion.

Once the solar wind is mediated strongly by pickup ions (the dashed curve, Figure 1), the newly born ions are much less energetic and no longer contribute as strongly to the temperature and pressure build-up in the outer heliosphere. Consequently, the outer heliosphere begins to cool, the inwardly directed pressure gradient is reduced, and the solar wind begins to revert to a less strongly mediated state. In the simulation, the periodic weak and strong mediation of the solar wind is very evident when the results are plotted in a movie format, and temperature fronts are seen to propagate continually out of the solar wind. This can be seen in the temperature sequence of Plate 1. The numerical simulations have been run for very long times, but no abatement of the temporal behaviour is observed. Essentially, the number density of neutrals entering the heliosphere is far too large to allow the solar wind to ever settle into a steady or quasi-steady state. The large neutral number density forces the wind to deviate strongly from its zeroth-order

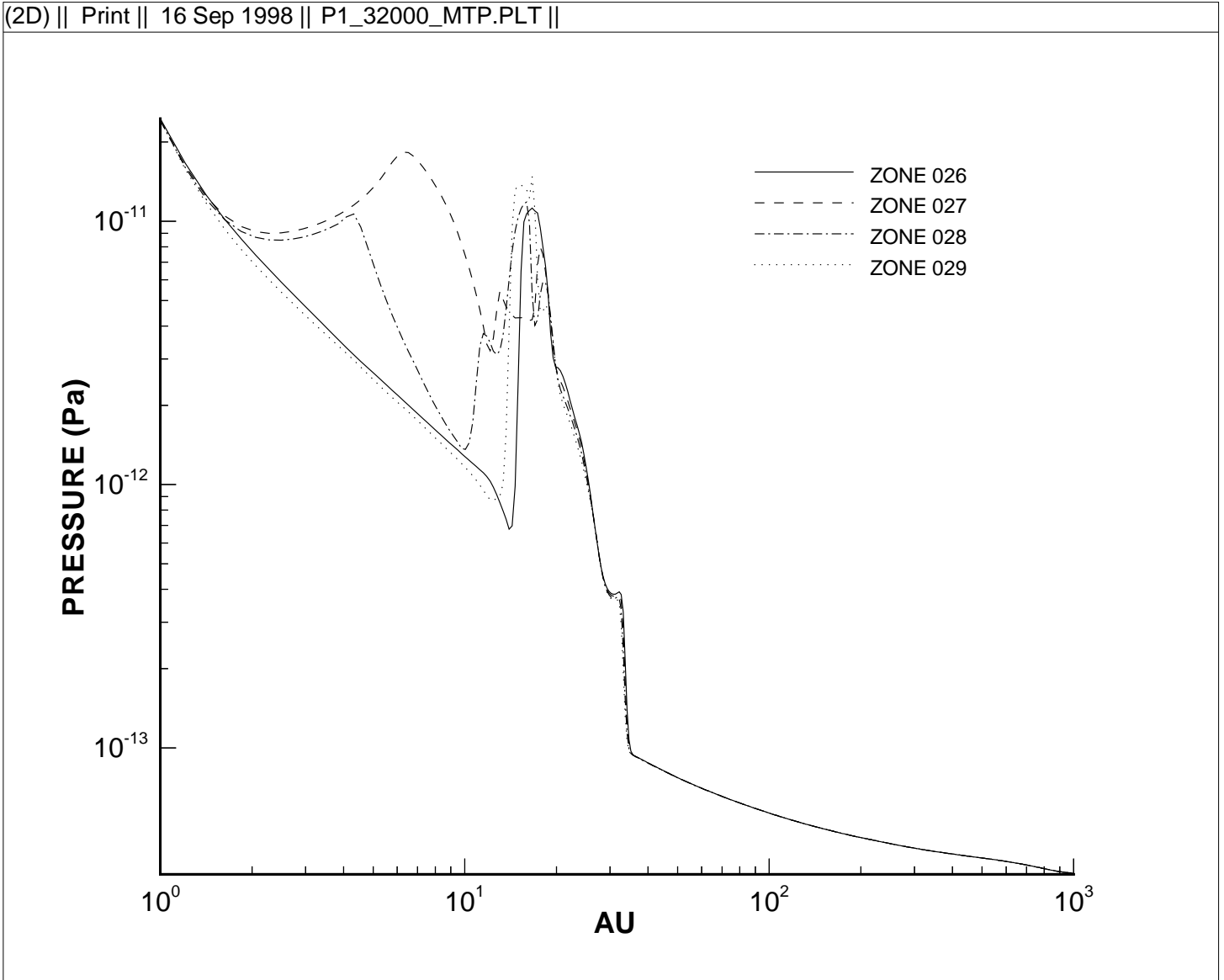


Fig. 5.— **Figure 3:** The plasma pressure along the stagnation axis. As in Figure 1, four curves are plotted, each of which corresponds to a figure from Plate 1 and the same line convention is followed as in Figure 1.

unmediated state, which in turn drives strong variations in the heating effects introduced by pickup ions.

Associated with the periodic increase of plasma temperature in the outer heliosphere is a decrease of the solar wind Mach number. The Mach number, which decreases in a pickup ion mediated solar wind because of both the solar wind deceleration and the increased sound speed, normally remains larger than 1 (supersonic). However, the strongly mediated solar wind Mach number decreases to 1 and less (Figure 1d). In this case, a termination shock is no longer necessary to bound the solar wind and a shock-free transition from supersonic to subsonic flow occurs (Plate 1b). As the outer heliospheric temperature begins to decrease again, the Mach number increases and a termination shock is again present. The sequence showing the presence of a termination shock, then a shock-free transition, followed by the reformation of the termination shock is exhibited in Plate 1A, B, and C respectively.

Finally, it should be noted that the heliopause region is unstable to a Rayleigh-Taylor-like instability. This is discussed in more detail in Zank (1998b) but the effect is understood easily. The coupling of neutral interstellar H to plasma introduces a frictional term proportional to $\langle\sigma v\rangle N\rho(\mathbf{u} - \mathbf{V}_n)$ in the momentum balance, where $\langle\sigma v\rangle$ denotes the charge exchange cross-section, N the neutral number density, \mathbf{V}_n the neutral velocity, and ρ and \mathbf{u} the plasma variables density and velocity. This expression is somewhat simplified compared to the full expressions used in the simulation. The inwardly directed frictional term plays a similar role as the gravitational term in the classical Rayleigh-Taylor analysis (e.g. Chandrasekhar 1961) and the charge-exchange ion-neutral friction term can therefore destabilize the heliopause. This leads to a somewhat unstable flow pattern in the upstream region, and some mixing of the solar wind and interstellar plasma.

In Plate 2, the global neutral distribution is also time-dependent but much more weakly than the plasma. Plate 2 suggests that the overall structure of the heliospheric hydrogen wall does not change very significantly with time.

4. Discussion and Conclusions

It is shown in this paper, using a coupled time-dependent system of hydrodynamic equations to describe the interaction between the heliosphere and a partially ionized interstellar cloud, that the configuration of the heliosphere and the interplanetary environment of the Earth are sensitive to the density of neutrals in the interstellar cloud surrounding the Sun. Raising the neutral number density in the surrounding cloud to $\sim 10 \text{ cm}^{-3}$, and leaving the other parameters at current values, has a dramatic effect on the global spatial and temporal structure of the heliosphere. The heliosphere in the upstream direction is reduced in extent to $\sim 10\text{--}14 \text{ au}$, compared to $\sim 80 - \sim 120 \text{ au}$ currently. Interstellar H^0 is filtered considerably as it enters the heliosphere, but some survives to penetrate successfully to 1 au where interstellar H^0 densities are $\sim 2 \text{ cm}^{-3}$, unlike the current conditions for which interstellar hydrogen is ionized entirely a few au from the Sun.

Although we have changed only the density of the surrounding cloud in these simulations, denser interstellar clouds are expected to have somewhat higher magnetic field strengths than the low value found locally. An average value of $7.3\mu\text{G}$ has been found recently for neutral interstellar gas from Zeeman splitting (Murphy and Lockman 1997). Were the interstellar magnetic field strength also to be increased to $7\mu\text{G}$ in our simulations, we would expect the heliopause radius to decrease possibly to a half to a third (depending on magnetic field orientation) of our computed radius, using a very crude balance estimate.

The heliospheric configuration becomes unstable; properties of the solar wind in the outer heliosphere vary on timescales as short as $\sim 66 \text{ days}$, and the termination shock disappears at times. The formation, disappearance and reformation of the termination shock appears to be periodic with a timescale of $\sim 280 \text{ days}$. Pickup ions dominate the thermodynamical character of the outer heliospheric solar wind completely. Solar wind temperatures, when pickup ions are included, can exceed 10^5 K . An inward pressure gradient can develop, which causes the solar wind to decelerate far more than predicted by simple mass-loading arguments and, consequently, the density decrease with increasing heliocentric distance can deviate from the usual r^{-2} dependence.

The implications of high interstellar neutral densities at 1 au for the terrestrial environment are interesting (e.g., Begelman and Rees, 1976; Bzowski et al. 1996). Is there evidence that the Earth has passed through a dense interstellar cloud in the (pre-)historical past, or might do so in the near future? A cloud condensation with density $\sim 10 \text{ cm}^{-3}$ embedded in the interstellar cloud complex flowing past the solar system could have a thickness of up to 0.3 pc and not violate any known observational constraints. Such a condensation would pass over the solar system in less than 15,000 years. There are several sets of data that indicate that the galactic environment of the Sun may have changed recently. The first set are geological records of nitrate layers ~ 11000 years before present, which have been attributed to energetic photons released by the Vela supernova explosion (Brakenridge 1981; also see Frisch and Slavin 1996). The second set of data is absorption line measurements of a slightly denser and cooler interstellar cloud seen within 3 pc of the Sun towards the stars ϵ CMA and α CMA in the anti-apex direction (see the discussion of the distribution of the nearby ISM in Frisch 1997b). The second cloud at $\sim -17 \text{ km s}^{-1}$ (heliocentric velocity, sometimes referred to as the “blue-shifted” cloud) has an electron density $n(e^-) \sim 0.4 \text{ cm}^{-3}$, and temperature $T=3600 \text{ K}$, in comparison with the values $\sim 0.1\text{--}0.2 \text{ cm}^{-3}$ and 7000 K seen locally (Gry and Dupin 1996, Lallement et al. 1994).

A third kind evidence is the cosmic ray record implied by the spikes in the ^{10}Be record found in Antarctic ice core samples at ages corresponding to 33 000 and 60 000 years ago (the D1 and D2 events respectively). Raisbeck et al. (1987) and Sonett et al. (1987) suggest that an increase in the cosmic ray flux on the Earth’s atmosphere can lead to an enhancement in the precipitated beryllium. Since supernova remnant shocks are thought to be responsible for accelerating galactic cosmic rays up to energies of $\sim 10^{14} \text{ eV}$ per nuclei, Sonett et al. suggested that the spikes might correspond to the passage of supernova shocks through the heliosphere. However, Frisch (1997a) has argued that little observational evidence in the LISM exists for the presence of a supernova shock at the times needed to explain the ^{10}Be enhancements. We suggest below an alternative interpretation of the ^{10}Be enhancements.

There are two possible ways that the cosmic ray flux at 1 au can be increased by the

interaction of the solar wind with a dense interstellar cloud. The first is that the increased pickup ion population increases the anomalous cosmic ray population. The second is that the reduction in the size of the heliospheric cavity indicates that galactic cosmic rays are no longer modulated significantly by an extended solar wind and so, at 1 au, the Earth samples the full spectrum. A more quantitative connection between the anomalous cosmic ray flux and a high density neutral interstellar cloud can be made using the model discussed above. The pickup ion number density at the termination shock, located at $\sim 10 - 14$ au, may be estimated as $n_{PI}(10\text{au}) \simeq 3 \times 10^{-2} \text{ cm}^{-3}$ (after solving $1/r^2 d/dr(r^2 u n_{PI}) = \langle \sigma v \rangle N_H n_{SW}$, under the assumptions that the solar wind number density $n_{SW} \simeq n_0 (r_0/r)^2$ on average, $\langle \sigma v \rangle \simeq 10^{-15} \text{ cm}^2$, and using Figure 2a). The injection of pickup ions into the anomalous cosmic ray component at a quasi-perpendicular termination shock has been considered by Zank et al. (1996c) and Lee et al. (1996). On the basis of such a shock “surfing”, or multiply reflected ion acceleration mechanism, Zank et al. estimated an injection efficiency of $\sim 20\%$ for hydrogen, with correspondingly smaller values for the heavier pickup ions. Thus, the number density of anomalous cosmic rays at 10 au for a heliosphere embedded in a H^0 interstellar cloud of density 10 cm^{-3} is $\sim 6 \times 10^{-3} \text{ cm}^{-3}$. To determine the cosmic ray density at 1 au, we can use a simple convection-diffusion solution to the cosmic ray transport equation, $n_{CR}(r\text{au}) = n_{CR}(10\text{au}) \exp[-u(10 - r)/\kappa_{rr}]$ where κ_{rr} is the radial diffusion coefficient for cosmic rays in the heliosphere. Using an estimate for the radial mean free path $\lambda_{rr} \sim 0.01$ au for 100 MV rigidity ions (Zank et al. 1998) yields $n_{CR}(1\text{au}) \sim 10^{-4} \text{ cm}^{-3}$. This is a very high level indeed. With such a large flux of anomalous cosmic rays incident on the atmosphere of the Earth, one might therefore expect a noticeable enhancement in the ^{10}Be flux measured on Earth. This effect will be further enhanced by the reduced modulation of galactic cosmic rays in the smaller heliosphere.

This alternative explanation for the ^{10}Be spikes offers a natural explanation for the absence of ^{10}Be enhancements prior to the D2 event in terms of the recent history of the galactic environment of the Sun (Frisch 1997b, Frisch 1998). During those periods when the heliosphere is embedded in an interstellar cloud with appreciable densities of H^0 , the anomalous and galactic cosmic ray fluxes incident on the Earth’s atmosphere will increase and enhance the level of precipitated ^{10}Be .

During the time prior to the D2 event (60 000 years ago), the Sun was in the third-quadrant void where the heliosphere would have been at least as large as today (Frisch 1998), entering the Local Fluff cloud complex only within the last $\sim 10^5$ years.

The effect of a large population of H° atoms filling interplanetary space at 1 au may well affect the interaction of the terrestrial magnetosphere with the solar wind, since interstellar He° densities will increase to $\sim 1 \text{ cm}^{-3}$ at 1 au for this increased density case and be comparable to the density of interstellar H° atoms. In addition, enhanced cosmic ray fluxes at 1 au may alter the global electric circuit, since the cosmic ray flux is the dominant source of conductivity in the lower atmosphere (Roble 1985); the global electrical circuit has been postulated to play a role in the terrestrial climate (Tinsley 1994,1997).

GPZ is supported in part by an NSF Young Investigator Award ATM-9357861, an NSF award ATM-9713223, a NASA award NAG5-6469, a NASA Delaware Space Grant NGT5-40024, and JPL contract 959167. PCF acknowledges the support of NASA grants NAG 5-6405 and NAG 5-7007.

REFERENCES

- Baranov, V.B., and Y.G. Malama, 1993, *J. Geophys. Res.*, 98, 15 157
- Begelman, M.C., and Rees, M.J., 1976, *Nature*, 261, 198
- Brakenridge, G. R. 1981, *Icarus*, 46, 81
- Bzowski, M., H.J. Fahr, and D. Rucinski, 1996, *Icarus*, 124, 209
- Chandrasekhar, S., 1961, *Hydrodynamic and Hydromagnetic Stability*, Dover
- Dalgarno, A., 1960, *Proc. Phys. Soc.*, 75, 374
- Dieter, N. H., Welch, W. J., Romney, J. D. 1976, *ApJ*, 206, L113
- Fahr, H.J., 1968, *Astrophys. Space Sci.*, 2, 496
- Faison, M. D., Goss, W. M., Diamond, P. J. 1998, *A&A*, 192, 4616
- Frail, D. A., Weisberg, J. M., Cordes, J. M., Mathers, C. 1994, *ApJ*, 436, 144
- Frisch, P.C., 1993, *ApJ*, 407, 198
- Frisch, P.C., 1995, *Space Sci. Rev.*, 72, 499
- Frisch, P.C., 1996, *Space Sci. Rev.*, 78, 213
- Frisch, P.C., 1997b, Enrico Fermi Institute Preprint No. 97-23
- Frisch, P.C., 1997a, *Space Sci. Rev.*, in press.
- Frisch, P.C., 1998, to be published in *Planetary Systems – The Long View*, eds. L. M. Celnikier and J. Tran Than Van, Editions Frontieres.
- Frisch, P.C. and Slavin, J. D., 1996, *Space Sci. Rev.*, 78, 223
- Frisch, P. C., and York, D. G. 1986, *The Galaxy and the Solar System*, ed. R. Smoluchowski, J. Bahcall, and M. Matthews, Tucson, University of Arizona Press, 83

- Frisch, P., Dorschner, J., Geiss, J., Greenberg, M., Grün, E., Hoppe, P., Jones, A., Krätschmer, W., Landgraf, M., Linde, T., Morfill, G., Reach, W., Slavin, J., Svestka, J., Witt, A., Zank, G.P. 1998, ApJ, submitted
- Gry, C., and Dupin, O. 1996, in Science with the Hubble Space Telescope - II, p.472, P.Benvenuti, F.D.Macchetto and E.J.Schreier, eds.Proceedings of a workshop held in Paris Dec 4-8, 1995.
- Hall, D.T., 1992, PhD Thesis, Univ. Arizona
- Heiles, C. 1997, ApJ, 481, 193
- Holzer, T.E., 1972, J. Geophys. Res., 77, 5407
- Holzer, T.E., 1989, ARA&A, 27, 199
- Lallement, R., Bertin, P., Ferlet, R., Vidal-Madjar, A., and Bertaux, J.L. 1994, A&A, 286, 898
- Lee, M.A., Shapiro, V.D., and Sagdeev, R.Z., 1996, J. Geophys. Res., 101, 4777
- McCrea, W.H., 1975, Nature, 255, 607
- McKay, C.P., and Thomas, G.E., 1978, Geophys. Res. Lett., 5, 215
- Meyer, D. M. and Blades, J. C. 1996, ApJ, 464, L179
- Murphy, E.M., Lockman, F.J., 1997, AAS, 190, 1703
- Pauls, H.L., Zank, G.P., and Williams, L.L., 1995, J. Geophys. Res., 100, 21 595
- Raisbeck, G.M. et al., 1987, Nature, 326, 273
- Reid, G.C., Isaksen, I.S.A., Holzer, T.E., and Crutzen, P.J., 1976, Nature, 259, 177
- Roble, R. G. 1985, J. Geophys. Res., 90, 6000
- Scoville, N.Z., and Sanders, D.B., 1986, The Galaxy and the Solar System, ed. R. Smoluchowski, J. Bahcall, and M. Matthews, Tucson, University of Arizona Press, 69

Shapley, H. 1921, *J. Geology*, 29, 502

Sonett, C.P., Morfill, G.E., and Jokipii, J.R., 1987, *Nature*, 330, 458

Thaddeus, P., 1986, *The Galaxy and the Solar System*, ed. R. Smoluchowski, J. Bahcall, and M. Matthews, Tucson, University of Arizona Press, 69

Tinsley, B. A. 1997, *EOS*, 78, 341

Tinsley, B. A. 1994, *EOS*, 75, 369

Watson, J. K. and Meyer, D. M. 1996, *ApJ*, 473, L127

Williams, L.L., Hall, D.T., Pauls, H.L., and Zank, G.P., 1997, *ApJ*, 476, 366

Zank, G.P., 1998a, *Space Sci. Rev.*, in press

Zank, G.P., 1998b, *J. Geophys. Res.*, submitted

Zank, G.P., Pauls, H.L., Williams, L.L., and Hall, D.T., 1996a, *J. Geophys. Res.*, 101, 21 639

Zank, G.P., Pauls, H.L., Williams, L.L., and Hall, D.T., 1996b, in *Proc. of Solar Wind 8*, 599

Zank, G.P., Pauls, H.L., Cairns, I.H., and Webb, G.M., 1996c, *J. Geophys. Res.*, 101, 457

Zank, G.P., Matthaeus, W.H., Bieber, J.W., and Moraal, H., 1998, *J. Geophys. Res.*, 103, 2085

Figure Captions

Plate 1: A time sequence of the plasma temperature distribution. The color corresponds to the $\text{Log}[\text{Temperature}]$. The ordering A, B, C, D corresponds to a temporal separation from the preceding figure of ~ 66 days. The four figures show an approximately full evolutionary cycle which is repeated on a ~ 280 day period. See text for further details.

Plate 2: A time sequence (corresponding to that of Plate 1) of the global distribution of the neutral interstellar H density. The color refers to the density measured in cm^{-3} . The hydrogen wall in the upstream direction is clearly visible, as is the effective filtration of H as it enters the heliosphere.

Figure 1: The plasma density (A), velocity (B), temperature (C) and Mach number (D) along the stagnation axis. Four curves are presented on each graph, each corresponding to a cut through one of the figures of Plate 1. In each case, the solid line corresponds to Plate 1A, the dashed line to Plate 1B, the dash-dotted line to Plate 1C and the dotted line to Plate 1D.

Figure 2: The interstellar neutral density (A), velocity (B), temperature (C) and Mach number (D) along the stagnation axis. Four curves are presented on each graph, each corresponding to a cut through one of the figures of Plate 2. In each case, the solid line corresponds to Plate 2A, the dashed to Plate 2B, the dash-dotted to Plate 2C and the dotted to Plate 2D.

Figure 3: The plasma pressure along the stagnation axis. As in Figure 1, four curves are plotted, each of which corresponds to a figure from Plate 1 and the same line convention is followed as in Figure 1.

This figure "plate1.jpg" is available in "jpg" format from:

<http://arxiv.org/ps/astro-ph/9901279v1>

This figure "plate2.jpg" is available in "jpg" format from:

<http://arxiv.org/ps/astro-ph/9901279v1>